Detection of change in cancer breast tissues from fractal indicators:

A brief introduction

SCAM

Séminaire Cristolien d'Analyse Multifractal

January 23, 2025

Barbara Pascal

CompuMAINE:* K. Batchelder, A. Khalil, B. G. White

Laboratoire des Sciences du Numérique de Nantes: B. Pascal

Laboratoire de Physique ENSL: P. Abry, B. Audit, L. Davy, N. Pustelnik

* Computational Modeling, Analysis of Imagery and Numerical Experiments

Context and motivations

Breast cancer:

- most common cancer amongst women with ~ 1 over 8 diagnosed
- early detection is critical for the patient's survival

Breast cancer:

- most common cancer amongst women with ~ 1 over 8 diagnosed
- early detection is critical for the patient's survival

X-ray imaging: most used imaging technique yielding a so-called *mammogram*

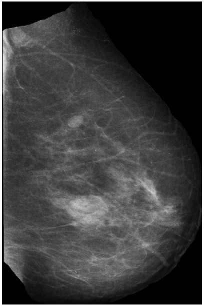

Breast cancer:

- most common cancer amongst women with $\sim$ 1 over 8 diagnosed
- early detection is critical for the patient's survival

X-ray imaging: most used imaging technique yielding a so-called *mammogram*

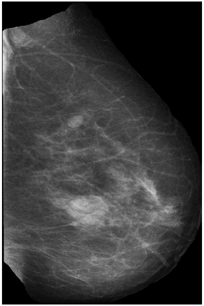

Assessment by a radiologist:

- fatty tissues: translucent to X-rays (black)
- epithelial and stromal tissues: absorb X-rays (white)
- tumorous tissues: **also absorb X-rays** (white)

$\Longrightarrow$ errors of both I and II types

Breast cancer:

- most common cancer amongst women with $\sim$ 1 over 8 diagnosed
- early detection is critical for the patient's survival

X-ray imaging: most used imaging technique yielding a so-called *mammogram*

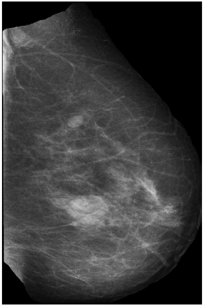

Assessment by a radiologist:

- fatty tissues: translucent to X-rays (black)
- epithelial and stromal tissues: absorb X-rays (white)
- tumorous tissues: **also absorb X-rays** (white)

$\Longrightarrow$ errors of both I and II types

Computer-Aided Detection: used in 92% of screening mammograms in the U.S.

Tissue density fluctuations in normal vs. cancerous breasts

Breast Imaging Reporting And Data System (BI-RADS): four categories

- `I`: Almost entirely fatty tissue (10% of women in U.S.)
- `II`: Scattered areas of density (40% of women in U.S.)
- `III`: Heterogeneous density (40% of women in U.S.)
- `IV`: Extremely dense (10% of women in U.S.)

(C. Balleyguier et al., 2007, Eur. J. Radiol.)

Tissue density fluctuations in normal vs. cancerous breasts

Breast Imaging Reporting And Data System (BI-RADS): four categories

- I: Almost entirely fatty tissue (10% of women in U.S.)
- II: Scattered areas of density (40% of women in U.S.)
- III: Heterogeneous density (40% of women in U.S.)
- IV: Extremely dense (10% of women in U.S.)

(C. Balleyguier et al., 2007, Eur. J. Radiol.)

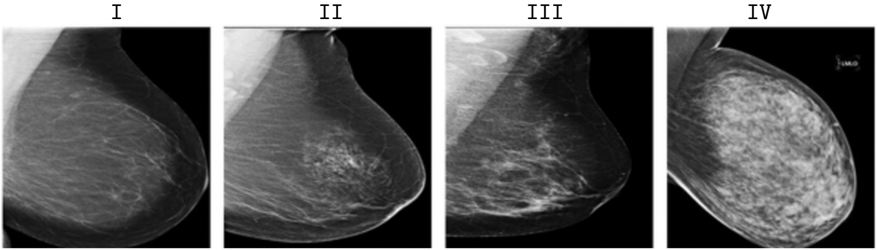

Source: B. White, 2023, *Electronic Theses and Dissertations, University of Maine*.

Tissue density fluctuations in normal vs. cancerous breasts

Breast Imaging Reporting And Data System (BI-RADS): four categories

- I: Almost entirely fatty tissue (10% of women in U.S.)
- II: Scattered areas of density (40% of women in U.S.)
- III: Heterogeneous density (40% of women in U.S.)
- IV: Extremely dense (10% of women in U.S.)

(C. Balleyguier et al., 2007, Eur. J. Radiol.)

I II III IV

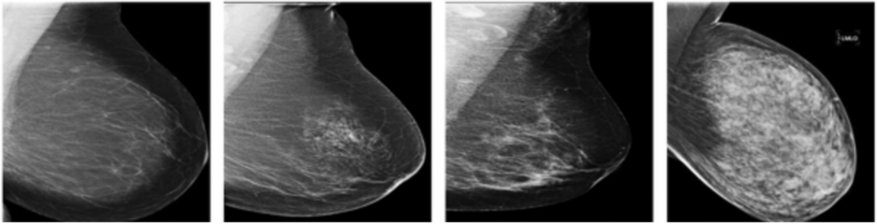

Source: B. White, 2023, *Electronic Theses and Dissertations, University of Maine*.

Overall mammographic density: (S. S. Nazari et al., 2018, *Breast cancer*)

$\Longrightarrow$ important risk factor for breast cancer radiological assessment

BI-RADS limitations:

- subjective, with both inter- and intra-observer variability
- classification in four classes not reflecting continuous changes in tissues

BI-RADS limitations:

- subjective, with both inter- and intra-observer variability
- classification in four classes not reflecting continuous changes in tissues

Self-similar isotropic random fields: $f(\boldsymbol{x}_0 + \lambda \boldsymbol{u}) - f(\boldsymbol{x}_0) \overset{\text{(law)}}{\simeq} \lambda^H (f(\boldsymbol{x}_0 + \boldsymbol{u}) - f(\boldsymbol{x}_0))$

Mammogram

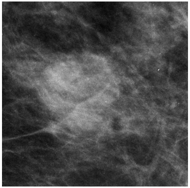

fractal random field

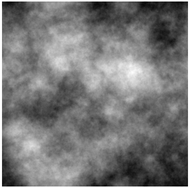

BI-RADS limitations:

- subjective, with both inter- and intra-observer variability
- classification in four classes not reflecting continuous changes in tissues

Self-similar isotropic random fields: $f(\boldsymbol{x}_0 + \lambda \boldsymbol{u}) - f(\boldsymbol{x}_0) \overset{\text{(law)}}{\simeq} \lambda^H \left(f(\boldsymbol{x}_0 + \boldsymbol{u}) - f(\boldsymbol{x}_0)\right)$

Mammogram

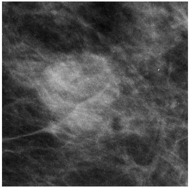

fractal random field

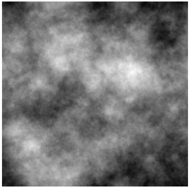

Self-similar textures: fractal analysis, e.g., fractal dimension of a rough surface, for

- classification of mammogram density (Caldwell et al., 1990, *Phys. Med. Biol.*)
- lesion detection in mammograms (Burgess et al., 2001, *Med. Biol.*)
- assessment of breast cancer risk (Heine et al., 2002, *Acad. Radiol.*)

Physiological motivations and goals

Breast **microenvironment** plays a crucial role in tumorigenesis:

- structure integrity preserved $\Longrightarrow$ lesions are suppressed
- structure lost by tissue disruption $\Longrightarrow$ tumor is promoted

Tumor vs. healthy not only in tumor but more fundamentally in surrounding tissue

Physiological motivations and goals

Breast **microenvironment** plays a crucial role in tumorigenesis:

- structure integrity preserved $\Longrightarrow$ lesions are suppressed
- structure lost by tissue disruption $\Longrightarrow$ tumor is promoted

Tumor vs. healthy not only in tumor but more fundamentally in surrounding tissue

Pioneer work: Marin et al., 2017, *Med. Phys.* quantitatively and objectively assessed

- tissue disruption
- loss of homeostasis in breast tissue microenvironment
- bilateral asymmetry

via wavelet-based mammogram local analysis.

Physiological motivations and goals

Breast **microenvironment** plays a crucial role in tumorigenesis:

- structure integrity preserved $\Longrightarrow$ lesions are suppressed
- structure lost by tissue disruption $\Longrightarrow$ tumor is promoted

Tumor vs. healthy not only in tumor but more fundamentally in surrounding tissue

Pioneer work: Marin et al., 2017, *Med. Phys.* quantitatively and objectively assessed

- tissue disruption
- loss of homeostasis in breast tissue microenvironment
- bilateral asymmetry

via wavelet-based mammogram local analysis.

Main idea: quantify density fluctuations through the Hölder exponent $h(\boldsymbol{x}_0)$ probed via

multifractal formalism based on 2D Wavelet Transform Modulus Maxima

$\Longrightarrow$ risk assessment and tumorous breasts detection without seeing a tumor

fBf of Hurst exponent $H \in [0,1]$ denoted $\{B_H(\boldsymbol{x}),\, \boldsymbol{x} \in \mathbb{R}^2\}$

- Gaussian field with zero-mean
- and for some $\sigma^2 > 0$, correlation function writing

$$\mathbb{E}\left[B_H(\boldsymbol{x})B_H(\boldsymbol{y})\right] = \frac{\sigma^2}{2}\left(\|\boldsymbol{x}\|^{2H} + \|\boldsymbol{y}\|^{2H} - \|\boldsymbol{x}-\boldsymbol{y}\|^{2H}\right)$$

fBf of Hurst exponent $H \in [0,1]$ denoted $\{B_H(\boldsymbol{x}),\, \boldsymbol{x} \in \mathbb{R}^2\}$

- Gaussian field with zero-mean
- and for some $\sigma^2 > 0$, correlation function writing

$$\mathbb{E}\left[B_H(\boldsymbol{x})B_H(\boldsymbol{y})\right] = \frac{\sigma^2}{2}\left(\|\boldsymbol{x}\|^{2H} + \|\boldsymbol{y}\|^{2H} - \|\boldsymbol{x}-\boldsymbol{y}\|^{2H}\right)$$

Stationary increments

$$\begin{aligned}\forall \boldsymbol{u} \in \mathbb{R}^2, \quad & \mathbb{E}\left[(B_H(\boldsymbol{x}+\boldsymbol{u}) - B_H(\boldsymbol{x}))(B_H(\boldsymbol{y}+\boldsymbol{u}) - B_H(\boldsymbol{y}))\right] \\ & = \|\boldsymbol{x}+\boldsymbol{u}-\boldsymbol{y}\|^{2H} + \|\boldsymbol{x}-\boldsymbol{u}-\boldsymbol{y}\|^{2H} - 2\|\boldsymbol{x}-\boldsymbol{y}\|^{2H}\end{aligned}$$

fBf of Hurst exponent $H \in [0,1]$ denoted $\{B_H(\boldsymbol{x}),\, \boldsymbol{x} \in \mathbb{R}^2\}$

- Gaussian field with zero-mean
- and for some $\sigma^2 > 0$, correlation function writing

$$\mathbb{E}\left[B_H(\boldsymbol{x})B_H(\boldsymbol{y})\right] = \frac{\sigma^2}{2}\left(\|\boldsymbol{x}\|^{2H} + \|\boldsymbol{y}\|^{2H} - \|\boldsymbol{x}-\boldsymbol{y}\|^{2H}\right)$$

Stationary increments

$$\begin{aligned}\forall \boldsymbol{u} \in \mathbb{R}^2, \quad & \mathbb{E}\left[(B_H(\boldsymbol{x}+\boldsymbol{u}) - B_H(\boldsymbol{x}))(B_H(\boldsymbol{y}+\boldsymbol{u}) - B_H(\boldsymbol{y}))\right] \\ & = \|\boldsymbol{x}+\boldsymbol{u}-\boldsymbol{y}\|^{2H} + \|\boldsymbol{x}-\boldsymbol{u}-\boldsymbol{y}\|^{2H} - 2\|\boldsymbol{x}-\boldsymbol{y}\|^{2H}\end{aligned}$$

For $\|\boldsymbol{u}\| \ll \|\boldsymbol{x}-\boldsymbol{y}\|$, $\quad \mathbb{E}\left[(B_H(\boldsymbol{x}+\boldsymbol{u}) - B_H(\boldsymbol{x}))(B_H(\boldsymbol{y}+\boldsymbol{u}) - B_H(\boldsymbol{y}))\right]$

$$= \|\boldsymbol{x}-\boldsymbol{y}\|^{2(H-1)} 2H(2H-1)\|\boldsymbol{u}\|^2 + o\left(\|\boldsymbol{u}\|^2\right)$$

A very short reminder about fractional Brownian fields

fBf of Hurst exponent $H \in [0,1]$ denoted $\{B_H(\boldsymbol{x}),\ \boldsymbol{x} \in \mathbb{R}^2\}$

- Gaussian field with zero-mean
- and for some $\sigma^2 > 0$, correlation function writing

$$\mathbb{E}\left[B_H(\boldsymbol{x})B_H(\boldsymbol{y})\right] = \frac{\sigma^2}{2}\left(\|\boldsymbol{x}\|^{2H} + \|\boldsymbol{y}\|^{2H} - \|\boldsymbol{x}-\boldsymbol{y}\|^{2H}\right)$$

Stationary increments

$$\forall \boldsymbol{u} \in \mathbb{R}^2, \quad \mathbb{E}\left[(B_H(\boldsymbol{x}+\boldsymbol{u}) - B_H(\boldsymbol{x}))(B_H(\boldsymbol{y}+\boldsymbol{u}) - B_H(\boldsymbol{y}))\right]$$
$$= \|\boldsymbol{x}+\boldsymbol{u}-\boldsymbol{y}\|^{2H} + \|\boldsymbol{x}-\boldsymbol{u}-\boldsymbol{y}\|^{2H} - 2\|\boldsymbol{x}-\boldsymbol{y}\|^{2H}$$

For $\|\boldsymbol{u}\| \ll \|\boldsymbol{x}-\boldsymbol{y}\|$, $\quad \mathbb{E}\left[(B_H(\boldsymbol{x}+\boldsymbol{u}) - B_H(\boldsymbol{x}))(B_H(\boldsymbol{y}+\boldsymbol{u}) - B_H(\boldsymbol{y}))\right]$

$$= \|\boldsymbol{x}-\boldsymbol{y}\|^{2(H-1)} 2H(2H-1)\|\boldsymbol{u}\|^2 + o\left(\|\boldsymbol{u}\|^2\right)$$

- $H < 1/2$: anti-correlated
- $H = 1/2$: uncorrelated $\Longrightarrow$ disruption
- $H > 1/2$: long-range correlated

Self-similarity

$$\forall \boldsymbol{x}_0 \in \mathbb{R}^2, \lambda > 0, \quad B_H(\boldsymbol{x}_0 + \lambda \boldsymbol{x}) - B_H(\boldsymbol{x}_0) \overset{\text{(law)}}{\simeq} \lambda^H (B_H(\boldsymbol{x}_0 + \boldsymbol{x}) - B_H(\boldsymbol{x}_0)) \ in\, \mathcal{V}(\boldsymbol{x}_0)$$

Self-similarity

$$\forall \boldsymbol{x}_0 \in \mathbb{R}^2, \lambda > 0, \quad B_H(\boldsymbol{x}_0 + \lambda \boldsymbol{x}) - B_H(\boldsymbol{x}_0) \overset{\text{(law)}}{\simeq} \lambda^H (B_H(\boldsymbol{x}_0 + \boldsymbol{x}) - B_H(\boldsymbol{x}_0)) \; in \, \mathcal{V}(\boldsymbol{x}_0)$$

The larger the Hurst exponent H, the smoother the texture.

`I`: fatty tissues

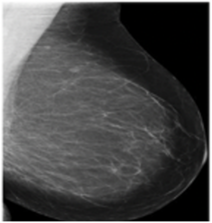

$H \simeq 0.30$

`IV`: dense tissues

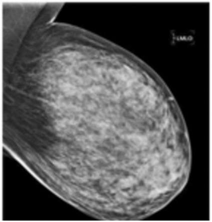

$H \simeq 0.65$

(Kestener et al., 2001, *Image Anal. Stereol.*)

CompuMAINE local mammogram analysis (Marin et al., 2017, *Phys. Med. Biol.*)

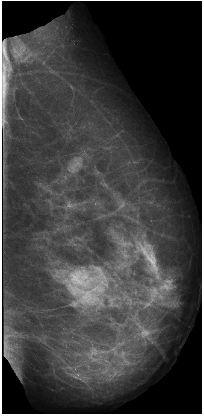

CompuMAINE local mammogram analysis (Marin et al., 2017, *Phys. Med. Biol.*)

- $H < 1/2$ monofractal anti-correlated: fatty tissues (healthy)

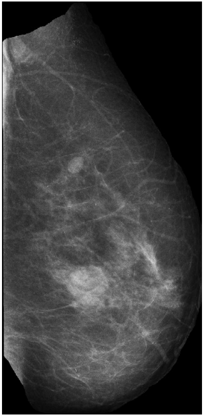

CompuMAINE local mammogram analysis (Marin et al., 2017, *Phys. Med. Biol.*)

- $H < 1/2$ monofractal anti-correlated: fatty tissues (healthy)
- $H > 1/2$ monofractal long-range correlated: dense tissues (healthy)

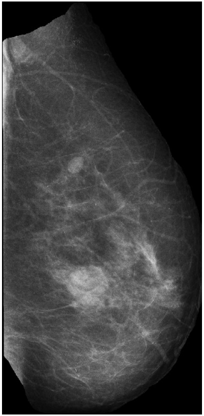

CompuMAINE local mammogram analysis (Marin et al., 2017, *Phys. Med. Biol.*)

- $H < 1/2$ monofractal anti-correlated: fatty tissues (healthy)
- $H > 1/2$ monofractal long-range correlated: dense tissues (healthy)
- $H \simeq 1/2$ monofractal uncorrelated: disrupted tissues (tumorous)

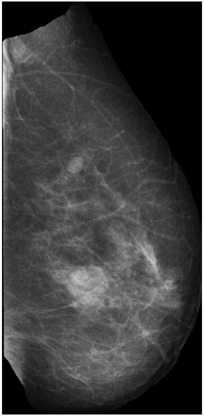

CompuMAINE local mammogram analysis (Marin et al., 2017, *Phys. Med. Biol.*)

- $H < 1/2$ monofractal anti-correlated: fatty tissues (healthy)
- $H > 1/2$ monofractal long-range correlated: dense tissues (healthy)
- $H \simeq 1/2$ monofractal uncorrelated: disrupted tissues (tumorous)

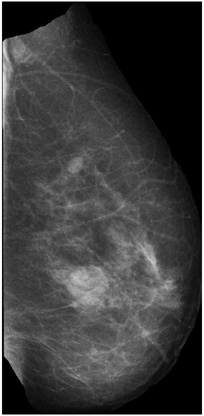

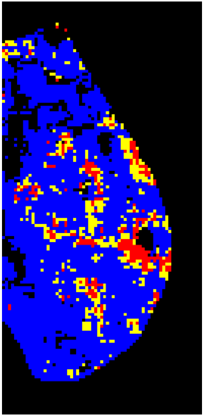

Assessment of the role of disruption in tumor promotion

Dataset: *University of South Florida*, Digital Database for Screening Mammography

- Mediolateral oblique views only;
- 43 normal, 49 cancer, 35 benign;
- for benign and cancer microcalcification only, masses excluded;

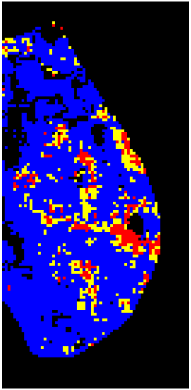

Image sliding-window analysis:

- squared 360×360-pixel window
- with 32-pixel horizontal and vertical shifts

$\Longrightarrow$ analysis of all 360×360-pixel overlapping patches

Example: mammogram of size 4459×2155 pixels

4457 patches $\Longleftrightarrow$ 4457 measures of the roughness H

Cancer risk metric: number of yellow patches

$H \sim 1/2$: disrupted tissues

$\Longrightarrow$ more **specific** than BI-RADS and **quantitative**

Assessment of the role of disruption in tumor promotion

Q.: Is the quantity of disrupted tissues, $H \simeq 1/2$, indicative of a tumorous breast?

Q.: Is the quantity of disrupted tissues, $H \simeq 1/2$, indicative of a tumorous breast?

Wilcoxon rank test a.k.a. Wilcoxon-Mann-Whitney

Independent sets of real numbers X and Y, of cardinalities n_x and n_y respectively

H0: $\mathbb{P}(X > Y) = \mathbb{P}(Y > X)$

Q.: Is the quantity of disrupted tissues, $H \simeq 1/2$, indicative of a tumorous breast?

Wilcoxon rank test a.k.a. Wilcoxon-Mann-Whitney

Independent sets of real numbers X and Y, of cardinalities n_x and n_y respectively

$$\textbf{H0}: \mathbb{P}(X > Y) = \mathbb{P}(Y > X)$$

(i) order elements of $X \cup Y$ to form an increasing sequence;

(ii) assign to each element in $X \cup Y$ its *rank* in the sequence;

(iii) sum the ranks of elements in X: variable S_x.

Q.: Is the quantity of disrupted tissues, $H \simeq 1/2$, indicative of a tumorous breast?

Wilcoxon rank test a.k.a. Wilcoxon-Mann-Whitney

Independent sets of real numbers X and Y, of cardinalities n_x and n_y respectively

$$\textbf{H0}: \mathbb{P}(X > Y) = \mathbb{P}(Y > X)$$

(i) order elements of $X \cup Y$ to form an increasing sequence;

(ii) assign to each element in $X \cup Y$ its *rank* in the sequence;

(iii) sum the ranks of elements in X: variable S_x.

If at least 20 samples, law of S_x well approximated by a Gaussian with

$$\mu = n_x n_y / 2; \quad \sigma^2 = n_x n_y (n_x + n_y + 1)/2.$$

If $|S_x - \mu|/\sigma > 1.96$, **H0** is rejected with confidence level $\alpha = 0.05$.

Assessment of the role of disruption in tumor promotion

Q.: Is the quantity of disrupted tissues, $H \simeq 1/2$, indicative of a tumorous breast?

Wilcoxon rank test a.k.a. Wilcoxon-Mann-Whitney

Independent sets of real numbers X and Y, of cardinalities n_x and n_y respectively

$$\textbf{H0}: \mathbb{P}(X > Y) = \mathbb{P}(Y > X)$$

(i) order elements of $X \cup Y$ to form an increasing sequence;

(ii) assign to each element in $X \cup Y$ its *rank* in the sequence;

(iii) sum the ranks of elements in X: variable S_x.

If at least 20 samples, law of S_x well approximated by a Gaussian with

$$\mu = n_x n_y / 2; \quad \sigma^2 = n_x n_y (n_x + n_y + 1)/2.$$

If $|S_x - \mu|/\sigma > 1.96$, **H0** is rejected with confidence level $\alpha = 0.05$.

Tumorous breasts have **more disrupted tissues**: normal vs. tumor: $P \sim 0.0006$

In details, normal vs. cancer: $P \sim 0.0023$, normal vs. benign: $P \sim 0.0049$.

Séminaire Cristolien d'Analyse Multifractale: February 4, 2021 *(online)*

bpascal-fr.github.io/assets/pdfs/SCAM21.pdf

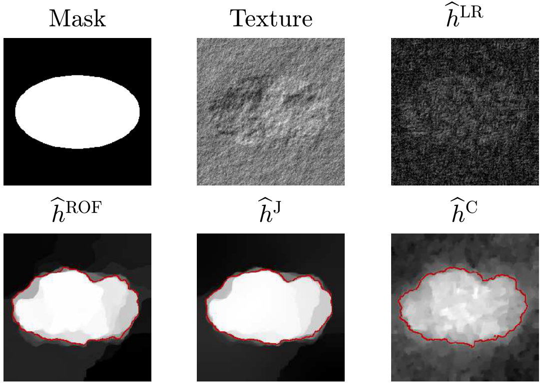

$\Longrightarrow$ estimation of local Hölder exponent $h(\boldsymbol{x})$ at the **pixel** level from **wavelet leaders**

(Pascal et al., 2020, *Ann. Telecommun.*; Pascal et al., 2021, *Appl. Comput. Harmon. Anal.*; Pascal et al., 2021, *J. Math. Imaging Vis.*)

But first: assess that **wavelet leaders formalism** agrees with UMaine analyzes

But first: assess that **wavelet leaders formalism** agrees with UMaine analyzes

Wavelet leaders: $\mathcal{L}_{a,\underline{n}}$ at scale a and pixel $\underline{n}$ supremum of wavelet coefficients

- at all finer scales $a' \leq a$
- in a spatial neighborhood

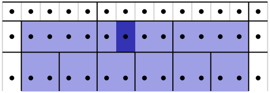

But first: assess that **wavelet leaders formalism** agrees with UMaine analyzes

Wavelet leaders: $\mathcal{L}_{a,\underline{n}}$ at scale a and pixel $\underline{n}$ supremum of wavelet coefficients

- at all finer scales $a' \leq a$
- in a spatial neighborhood

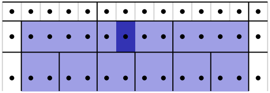

For a grid of pixels $\Omega \subset \mathbb{R}^2$, scaling exponent $\zeta(q)$ accessible through

$$\frac{1}{|\Omega|} \sum_{\underline{n} \in \Omega} \mathcal{L}_{a,\underline{n}}^{q} = F_q a^{\zeta(q)}, \quad a \to 0^+$$

homogeneous monofractal texture of Hurst exponent $H \Longrightarrow \zeta(q) = qH$

(Wendt et al., 2007, *IEEE Signal Process. Mag.*)

Patch-wise fractal analysis of mammographic breast tissue

But first: assess that **wavelet leaders formalism** agrees with UMaine analyzes

Wavelet leaders: $\mathcal{L}_{a,\underline{n}}$ at scale a and pixel $\underline{n}$ supremum of wavelet coefficients

- at all finer scales $a' \leq a$
- in a spatial neighborhood

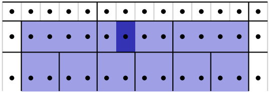

For a grid of pixels $\Omega \subset \mathbb{R}^2$, scaling exponent $\zeta(q)$ accessible through

$$\frac{1}{|\Omega|} \sum_{\underline{n} \in \Omega} \mathcal{L}_{a,\underline{n}}^{q} = F_q a^{\zeta(q)}, \quad a \to 0^{+}$$

homogeneous monofractal texture of Hurst exponent $H \Longrightarrow \zeta(q) = qH$

(Wendt et al., 2007, *IEEE Signal Process. Mag.*)

$\Longrightarrow$ linear regression to estimate H for all 360×360-pixel overlapping patches

Wavelet leader coefficients (Wendt et al., 2009, Sig. Process.)

- $H < 1/2$ monofractal anti-correlated: fatty tissues (healthy)
- $H > 1/2$ monofractal long-range correlated: dense tissues (healthy)
- $H \simeq 1/2$ monofractal uncorrelated: disrupted tissues (tumorous)

Wavelet leader coefficients (Wendt et al., 2009, Sig. Process.)

- $H < 1/2$ monofractal anti-correlated: fatty tissues (healthy)
- $H > 1/2$ monofractal long-range correlated: dense tissues (healthy)
- $H \simeq 1/2$ monofractal uncorrelated: disrupted tissues (tumorous)

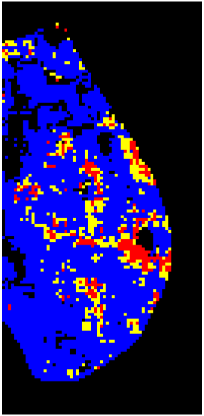

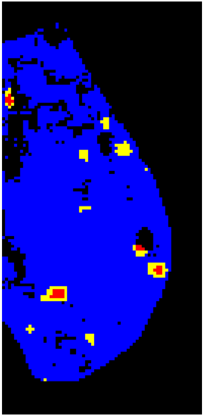

Wavelet leader coefficients (Wendt et al., 2009, Sig. Process.)

- $H < 1/2$ monofractal anti-correlated: fatty tissues (healthy)
- $H > 1/2$ monofractal long-range correlated: dense tissues (healthy)
- $H \simeq 1/2$ monofractal uncorrelated: disrupted tissues (tumorous)

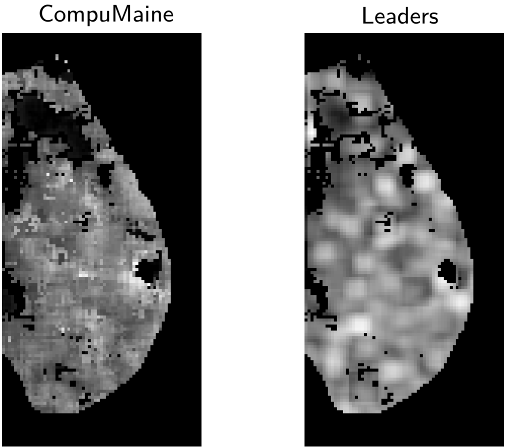

Multifractal formalism: **local** Hölder regularity $h(\boldsymbol{x}_0)$

$$|f(\boldsymbol{x}) - P_n(\boldsymbol{x} - \boldsymbol{x}_0)| \leq C|\boldsymbol{x} - \boldsymbol{x}_0|^{h(\boldsymbol{x}_0)} \quad \text{for } \boldsymbol{x} \in \mathcal{V}(\boldsymbol{x}_0)$$

with P_n a polynomial of degree $n < h(\boldsymbol{x}_0)$

Local isotropic scale invariance: $f(\boldsymbol{x}_0 + \lambda \boldsymbol{u}) - f(\boldsymbol{x}_0) \overset{\text{(law)}}{\simeq} \lambda^{h(\boldsymbol{x}_0)} (f(\boldsymbol{x}_0 + \boldsymbol{u}) - f(\boldsymbol{x}_0))$

Multifractal formalism: local Hölder regularity $h(\boldsymbol{x}_0)$

$$|f(\boldsymbol{x}) - P_n(\boldsymbol{x} - \boldsymbol{x}_0)| \leq C|\boldsymbol{x} - \boldsymbol{x}_0|^{h(\boldsymbol{x}_0)} \quad \text{for } \boldsymbol{x} \in \mathcal{V}(\boldsymbol{x}_0)$$

with P_n a polynomial of degree $n < h(\boldsymbol{x}_0)$

Local isotropic scale invariance: $f(\boldsymbol{x}_0 + \lambda \boldsymbol{u}) - f(\boldsymbol{x}_0) \overset{\text{(law)}}{\simeq} \lambda^{h(\boldsymbol{x}_0)} \left(f(\boldsymbol{x}_0 + \boldsymbol{u}) - f(\boldsymbol{x}_0)\right)$

For $h(x_0) \in (0, 1)$ and cusp-like only singularities

$h(x) \equiv h_1 = 0.9$ $\qquad$ $h(x) \equiv h_2 = 0.3$

Multifractal formalism: **local** Hölder regularity $h(\boldsymbol{x}_0)$

$$|f(\boldsymbol{x}) - P_n(\boldsymbol{x} - \boldsymbol{x}_0)| \leq C|\boldsymbol{x} - \boldsymbol{x}_0|^{h(\boldsymbol{x}_0)} \quad \text{for } \boldsymbol{x} \in \mathcal{V}(\boldsymbol{x}_0)$$

with P_n a polynomial of degree $n < h(\boldsymbol{x}_0)$

Local isotropic scale invariance: $f(\boldsymbol{x}_0 + \lambda \boldsymbol{u}) - f(\boldsymbol{x}_0) \overset{\text{(law)}}{\simeq} \lambda^{h(\boldsymbol{x}_0)} (f(\boldsymbol{x}_0 + \boldsymbol{u}) - f(\boldsymbol{x}_0))$

For $h(x_0) \in (0, 1)$ and cusp-like only singularities

$h(x) \equiv h_1 = 0.9$ $h(x) \equiv h_2 = 0.3$

Singularity spectrum: $\mathcal{D}(h)$ Haussdorff dimension of $\{\boldsymbol{x} \in \mathbb{R}^2, \, h(\boldsymbol{x}) = h\}$

For a monofractal field, e.g., fractional Brownian field B_H: $h(\boldsymbol{x}_0) \equiv H$ and

$$\mathcal{D}(h) = \begin{cases} 2 & h = H \\ -\infty & h \neq H \end{cases}$$

Multifractal analysis of mamographic microenvironment

Kestener et al., 2001; Marin et al., 2017; Gerasimova-Chechkina et al., 2021

Multifractal analysis of mamographic microenvironment

Kestener et al., 2001; Marin et al., 2017; Gerasimova-Chechkina et al., 2021

2D Wavelet Transform: $\{f(\boldsymbol{x}),\ \boldsymbol{x} \in \mathbb{R}^2\}$ 2D-field

Smoothing function $\varphi(\boldsymbol{x}) \Longrightarrow$ wavelets $\psi_1(\boldsymbol{x}) = \partial_{x_1}\varphi(x_1, x_2)$, $\psi_2(\boldsymbol{x}) = \partial_{x_2}\varphi(x_1, x_2)$

$$\mathbf{T}_\psi[f](\boldsymbol{b}, a) = \begin{pmatrix} a^{-2}\int \psi_1\left(a^{-1}(\boldsymbol{x}-\boldsymbol{b})\right) f(\boldsymbol{x})\,\mathrm{d}\boldsymbol{x} \\ a^{-2}\int \psi_2\left(a^{-1}(\boldsymbol{x}-\boldsymbol{b})\right) f(\boldsymbol{x})\,\mathrm{d}\boldsymbol{x} \end{pmatrix} \overset{\text{(complex)}}{=} \mathbf{M}_\psi[f](\boldsymbol{b}, a)\exp\left(\mathrm{i}\mathbf{A}_\psi[f](\boldsymbol{b}, a)\right)$$

Example: Gaussian and Mexican hat smoothing functions

$$\varphi_{\text{Gauss}}(\boldsymbol{x}) = \exp(-\|\boldsymbol{x}\|^2/2); \quad \varphi_{\text{Mex}}(\boldsymbol{x}) = (2 - \|\boldsymbol{x}\|^2)\exp(-\|\boldsymbol{x}\|^2/2)$$

leading respectively to $n_\psi = 1$ and $n_\psi = 3$ vanishing moments

Multifractal analysis of mamographic microenvironment

Kestener et al., 2001; Marin et al., 2017; Gerasimova-Chechkina et al., 2021

2D Wavelet Transform: $\{f(\boldsymbol{x}),\ \boldsymbol{x} \in \mathbb{R}^2\}$ 2D-field

Smoothing function $\varphi(\boldsymbol{x}) \Longrightarrow$ wavelets $\psi_1(\boldsymbol{x}) = \partial_{x_1}\varphi(x_1, x_2)$, $\psi_2(\boldsymbol{x}) = \partial_{x_2}\varphi(x_1, x_2)$

$$\mathbf{T}_\psi[f](\boldsymbol{b}, a) = \begin{pmatrix} a^{-2}\int \psi_1\left(a^{-1}(\boldsymbol{x}-\boldsymbol{b})\right) f(\boldsymbol{x})\,\mathrm{d}\boldsymbol{x} \\ a^{-2}\int \psi_2\left(a^{-1}(\boldsymbol{x}-\boldsymbol{b})\right) f(\boldsymbol{x})\,\mathrm{d}\boldsymbol{x} \end{pmatrix} \overset{\text{(complex)}}{=} \mathbf{M}_\psi[f](\boldsymbol{b}, a)\exp\left(\mathrm{i}\mathbf{A}_\psi[f](\boldsymbol{b}, a)\right)$$

Example: Gaussian and Mexican hat smoothing functions

$$\varphi_{\text{Gauss}}(\boldsymbol{x}) = \exp(-\|\boldsymbol{x}\|^2/2); \quad \varphi_{\text{Mex}}(\boldsymbol{x}) = (2 - \|\boldsymbol{x}\|^2)\exp(-\|\boldsymbol{x}\|^2/2)$$

leading respectively to $n_\psi = 1$ and $n_\psi = 3$ vanishing moments

Wavelet Transform Modulus Maxima

$$\{(\boldsymbol{b}, a) \in \mathbb{R}^2, \times\mathbb{R}_+^* \quad \mathbf{M}_\psi[f](\boldsymbol{b}, a) \text{ locally maximal in direction } \mathbf{A}_\psi[f](\boldsymbol{b}, a)\}$$

Multifractal analysis using Wavelet Transform Modulus Maxima

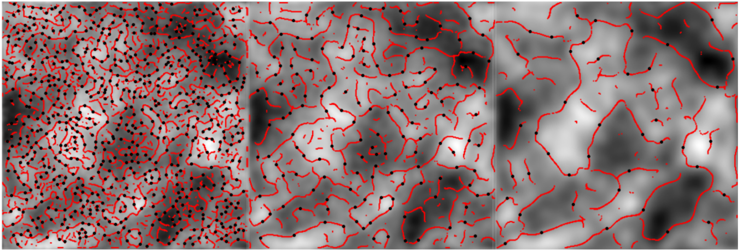

Figure 4.2: The maxima chains are shown for scales $a = 2^1\sigma_w$ (left), $a = 2^2\sigma_w$ (middle), and $a = 2^3\sigma_w$ (right) (where $\sigma_w = 7$ pixels) overlaid onto a 2D fBm image with $H = 0.5$. The local maxima along $\mathcal{M}_\psi$ (WTMMM) are shown through small filled black dots.

Source: Basel G. White

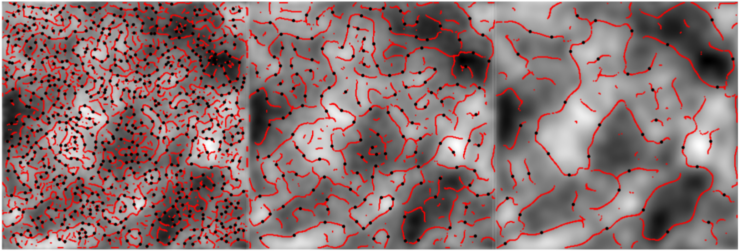

Figure 4.2: The maxima chains are shown for scales $a = 2^1\sigma_w$ (left), $a = 2^2\sigma_w$ (middle), and $a = 2^3\sigma_w$ (right) (where $\sigma_w = 7$ pixels) overlaid onto a 2D fBm image with $H = 0.5$. The local maxima along $\mathcal{M}_\psi$ (WTMMM) are shown through small filled black dots.

Source: Basel G. White

Wavelet Transform space-scale skeleton: $\mathcal{L}(a)$

lines formed by WTMM maxima across scales

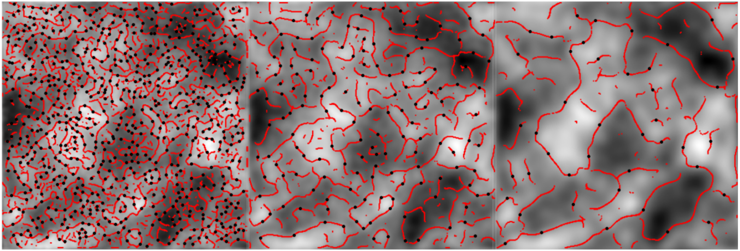

Figure 4.2: The maxima chains are shown for scales $a = 2^1\sigma_w$ (left), $a = 2^2\sigma_w$ (middle), and $a = 2^3\sigma_w$ (right) (where $\sigma_w = 7$ pixels) overlaid onto a 2D fBm image with $H = 0.5$. The local maxima along $\mathcal{M}_\psi$ (WTMMM) are shown through small filled black dots.

Source: Basel G. White

Wavelet Transform space-scale skeleton: $\mathcal{L}(a)$

lines formed by WTMM maxima across scales

If a maxima line $\mathcal{L}_{\boldsymbol{x}_0}(a)$ is pointing toward a singularity $\boldsymbol{x}_0$ as $a \to 0^+$, then

$$\mathbf{M}_\psi[f](\mathcal{L}_{\boldsymbol{x}_0}(a)) \sim a^{h(\boldsymbol{x}_0)}, \quad a \to 0^+$$

provided that the wavelet has $n_\psi > h(\boldsymbol{x}_0)$ vanishing moments.

Partition function: for a set $\mathfrak{L}(a)$ of maxima lines

$$\mathcal{Z}(q, a) = \sum_{\ell \in \mathfrak{L}(a)} \left(\sup_{(\boldsymbol{b}, a') \in \ell, a' \leq a} \mathbf{M}_\psi[f](\boldsymbol{b}, a') \right)^q$$

q: statistical order moment

Partition function: for a set $\mathfrak{L}(a)$ of maxima lines

$$\mathcal{Z}(q,a) = \sum_{\ell \in \mathfrak{L}(a)} \left(\sup_{(\boldsymbol{b},a') \in \ell, a' \leq a} \mathbf{M}_{\psi}[f](\boldsymbol{b},a') \right)^{q}$$

q: statistical order moment

Roughness, quantified by Hölder exponent, characterized by $\tau(q)$ spectrum

$$\mathcal{Z}(q,a) \sim a^{\tau(q)}, \quad a \to 0^{+}$$

For 2D fractional Brownian field: $\tau(q) = qH - 2$ is **linear**.

Partition function: for a set $\mathfrak{L}(a)$ of maxima lines

$$\mathcal{Z}(q,a) = \sum_{\ell \in \mathfrak{L}(a)} \left(\sup_{(\boldsymbol{b},a') \in \ell, a' \leq a} \mathbf{M}_\psi[f](\boldsymbol{b},a') \right)^q$$

q: statistical order moment

Roughness, quantified by Hölder exponent, characterized by $\tau(q)$ spectrum

$$\mathcal{Z}(q,a) \sim a^{\tau(q)}, \quad a \to 0^+$$

For 2D fractional Brownian field: $\tau(q) = qH - 2$ is **linear**.

Singularity spectrum: $\mathcal{D}(h)$ Haussdorff dimension of $\{\boldsymbol{x} \in \mathbb{R}^2,\ h(\boldsymbol{x}) = h\}$

$$\mathcal{D}(h) = \min_q \left(qh - \tau(q) \right) \quad \text{(Legendre transform of } \tau)$$

Numerically: unstable estimation of $\tau(q)$ and $\mathcal{D}(q)$

$\Longrightarrow$ Mean quantities in a canonical ensemble with Boltzmann weights

$$\mathrm{W}_\psi[f](q,\ell,a) = \frac{\left| \sup\limits_{(\boldsymbol{b},a')\in\ell, a'\leq a} \mathbf{M}_\psi[f](\boldsymbol{b},a') \right|^q}{\mathcal{Z}(q,a)}$$

Numerically: unstable estimation of $\tau(q)$ and $\mathcal{D}(q)$

$\Longrightarrow$ Mean quantities in a canonical ensemble with Boltzmann weights

$$\mathrm{W}_\psi[f](q,\ell,a) = \frac{\left|\sup_{(\boldsymbol{b},a')\in\ell,a'\leq a} \mathbf{M}_\psi[f](\boldsymbol{b},a')\right|^q}{\mathcal{Z}(q,a)}$$

Roughness: robust local regularity estimation

$$h(q,a) = \sum_{\ell\in\mathfrak{L}(a)} \ln\left(\left|\sup_{(\boldsymbol{b},a')\in\ell,a'\leq a} \mathbf{M}_\psi[f](\boldsymbol{b},a')\right|\right) \mathrm{W}_\psi[f](q,\ell,a),$$

$$h(q) = \frac{\mathrm{d}\tau}{\mathrm{d}q} = \lim_{a\to 0^+} \frac{h(q,a)}{\ln a}$$

Numerically: unstable estimation of $\tau(q)$ and $\mathcal{D}(q)$

$\Longrightarrow$ Mean quantities in a canonical ensemble with Boltzmann weights

$$\mathrm{W}_\psi[f](q,\ell,a) = \frac{\left|\sup_{(\boldsymbol{b},a')\in\ell, a'\leq a} \mathbf{M}_\psi[f](\boldsymbol{b},a')\right|^q}{\mathcal{Z}(q,a)}$$

Roughness: robust local regularity estimation

$$h(q,a) = \sum_{\ell\in\mathfrak{L}(a)} \ln\left(\left|\sup_{(\boldsymbol{b},a')\in\ell, a'\leq a} \mathbf{M}_\psi[f](\boldsymbol{b},a')\right|\right) \mathrm{W}_\psi[f](q,\ell,a),$$

$$h(q) = \frac{\mathrm{d}\tau}{\mathrm{d}q} = \lim_{a\to 0^+} \frac{h(q,a)}{\ln a}$$

Singularity spectrum:

$$\mathcal{D}(q,a) = \sum_{\ell\in\mathfrak{L}(a)} \ln\left(\mathrm{W}_\psi[f](q,\ell,a)\right) \mathrm{W}_\psi[f](q,\ell,a),$$

$$\mathcal{D}(q) = \lim_{a\to 0^+} \frac{\mathcal{D}(q,a)}{\ln a}$$

Patch-wise fractal analysis of mammographic breast tissue

Roughness: $h(q) = \lim_{a \to 0^+} \frac{h(q, a)}{\ln a}$; **Singularity spectrum:** $\mathcal{D}(q, a) = \lim_{a \to 0^+} \frac{\mathcal{D}(q, a)}{\ln a}$

- The larger the patch, the larger the range of q values, the better the estimate;
- but risk of confusing average of several monofractal signatures and multifractal.

$\Longrightarrow$ estimation on overlapping patches of size 360×360 pixels with 32-pixel shift

Roughness: $h(q) = \lim_{a \to 0^+} \frac{h(q, a)}{\ln a}$; **Singularity spectrum:** $\mathcal{D}(q, a) = \lim_{a \to 0^+} \frac{\mathcal{D}(q, a)}{\ln a}$

- The larger the patch, the larger the range of q values, the better the estimate;
- but risk of confusing average of several monofractal signatures and multifractal.

$\Longrightarrow$ estimation on overlapping patches of size 360×360 pixels with 32-pixel shift

Image sliding window analysis

1. Check that the central 256×256 pixels are contained in the mask;
2. if so, compute the Wavelet Transform for 50 scales, from $a = 7$ to 120 pixels;
3. extract the space-scale skeleton from the central 256×256 pixels;
4. compute $h(q, a)$ and $\mathcal{D}(q, a)$ from the partition function $\mathcal{Z}(q, a)$;
5. linear regressions $h(q, a)$ vs. $\log_2(a)$ and $\mathcal{D}(q, a)$ vs. $\log_2(a)$:

how to choose the range of scales $[a_{\min}, a_{\max}]$?

Patch-wise fractal analysis of mammographic breast tissue

For **each** patch of 360×360 pixels, i.e., 15.5×15.5 mm

$$\text{roughness: } h(q) = \lim_{a \to 0^+} \frac{h(q,a)}{\ln a}; \qquad \text{singularity spectrum: } \mathcal{D}(q,a) = \lim_{a \to 0^+} \frac{\mathcal{D}(q,a)}{\ln a}$$

$\Longrightarrow$ linear regressions $h(q,a)$ vs. $\log_2(a)$ and $\mathcal{D}(q,a)$ vs. $\log_2(a)$ across $[a_{\min}, a_{\max}]$

For **each** patch of 360×360 pixels, i.e., 15.5×15.5 mm

$$\text{roughness: } h(q) = \lim_{a \to 0^+} \frac{h(q,a)}{\ln a}; \qquad \text{singularity spectrum: } \mathcal{D}(q,a) = \lim_{a \to 0^+} \frac{\mathcal{D}(q,a)}{\ln a}$$

$\Longrightarrow$ linear regressions $h(q,a)$ vs. $\log_2(a)$ and $\mathcal{D}(q,a)$ vs. $\log_2(a)$ across $[a_{\min}, a_{\max}]$

The Autofit Methodology: imposing $\log_2 a_{\max} - \log_2 a_{\min} \geq 1$ explore

$$\log_2 \frac{a_{\min}}{\sigma_w} = 0.0, 0.1, \ldots, 2.1, \;, \;\; \log_2 \frac{a_{\max}}{\sigma_w} = 2.0, 2.1, \ldots, 4.1, \;\; \text{with} \;\; \sigma_w = 7 \text{ pixels}$$

and select $[a_{\min}, a_{\max}]$ if and only if

For **each** patch of 360 × 360 pixels, i.e., 15.5 × 15.5 mm

$$\text{roughness: } h(q) = \lim_{a\to 0^+} \frac{h(q,a)}{\ln a}; \quad \text{singularity spectrum: } \mathcal{D}(q,a) = \lim_{a\to 0^+} \frac{\mathcal{D}(q,a)}{\ln a}$$

$\Longrightarrow$ linear regressions $h(q,a)$ vs. $\log_2(a)$ and $\mathcal{D}(q,a)$ vs. $\log_2(a)$ across $[a_{\min}, a_{\max}]$

The Autofit Methodology: imposing $\log_2 a_{\max} - \log_2 a_{\min} \geq 1$ explore

$$\log_2 \frac{a_{\min}}{\sigma_w} = 0.0, 0.1, \ldots, 2.1, \;, \quad \log_2 \frac{a_{\max}}{\sigma_w} = 2.0, 2.1, \ldots, 4.1, \quad \text{with} \quad \sigma_w = 7 \text{ pixels}$$

and select $[a_{\min}, a_{\max}]$ if and only if

- linear regression on $h(q=0,a)$ from $a_{\min}$ to $a_{\max}$ yields

$$-0.2 < \widehat{h}(q=0) = \widehat{H} < 1$$

  - $H \leq -0.2$: high roughness $\Longrightarrow$ abnormally high noise
  - $H \geq 1$: low roughness, differentiable field $\Longrightarrow$ artificially smooth

For **each** patch of 360×360 pixels, i.e., 15.5×15.5 mm

roughness: $h(q) = \lim_{a \to 0^+} \frac{h(q,a)}{\ln a}$; singularity spectrum: $\mathcal{D}(q,a) = \lim_{a \to 0^+} \frac{\mathcal{D}(q,a)}{\ln a}$

$\Longrightarrow$ linear regressions $h(q,a)$ vs. $\log_2(a)$ and $\mathcal{D}(q,a)$ vs. $\log_2(a)$ across $[a_{\min}, a_{\max}]$

The Autofit Methodology: imposing $\log_2 a_{\max} - \log_2 a_{\min} \geq 1$ explore

$$\log_2 \frac{a_{\min}}{\sigma_w} = 0.0, 0.1, \ldots, 2.1, , \;\; \log_2 \frac{a_{\max}}{\sigma_w} = 2.0, 2.1, \ldots, 4.1, \;\; \text{with} \;\; \sigma_w = 7 \text{ pixels}$$

and select $[a_{\min}, a_{\max}]$ if and only if

- linear regression on $\mathcal{D}(q=0,a)$ from $a_{\min}$ to $a_{\max}$ yields

$$1.7 < \widehat{\mathcal{D}}(h(q=0)) < 2.5$$

for a monofractal field of Hurst exponent H, expected to be $\mathcal{D}(H) = 2$

but finite size effect affect the maxima lines as $a \to 0^+$

Patch-wise fractal analysis of mammographic breast tissue

For **each** patch of 360×360 pixels, i.e., 15.5×15.5 mm

$$\text{roughness: } h(q) = \lim_{a \to 0^+} \frac{h(q,a)}{\ln a}; \quad \text{singularity spectrum: } \mathcal{D}(q,a) = \lim_{a \to 0^+} \frac{\mathcal{D}(q,a)}{\ln a}$$

$\Longrightarrow$ linear regressions $h(q,a)$ vs. $\log_2(a)$ and $\mathcal{D}(q,a)$ vs. $\log_2(a)$ across $[a_{\min}, a_{\max}]$

The Autofit Methodology: imposing $\log_2 a_{\max} - \log_2 a_{\min} \geq 1$ explore

$$\log_2 \frac{a_{\min}}{\sigma_w} = 0.0, 0.1, \dots, 2.1, , \quad \log_2 \frac{a_{\max}}{\sigma_w} = 2.0, 2.1, \dots, 4.1, \quad \text{with} \quad \sigma_w = 7 \text{ pixels}$$

and select $[a_{\min}, a_{\max}]$ if and only if

- coefficient of determination of linear regression on $h(q=0,a)$ from $a_{\min}$ to $a_{\max}$

  $$R^2 > 0.96$$

  sufficiently linear to extract the Hurst exponent H

Patch-wise fractal analysis of mammographic breast tissue

For **each** patch of 360×360 pixels, i.e., 15.5×15.5 mm

$$\text{roughness: } h(q) = \lim_{a \to 0^+} \frac{h(q,a)}{\ln a}; \qquad \text{singularity spectrum: } \mathcal{D}(q,a) = \lim_{a \to 0^+} \frac{\mathcal{D}(q,a)}{\ln a}$$

$\Longrightarrow$ linear regressions $h(q,a)$ vs. $\log_2(a)$ and $\mathcal{D}(q,a)$ vs. $\log_2(a)$ across $[a_{\min}, a_{\max}]$

The Autofit Methodology: imposing $\log_2 a_{\max} - \log_2 a_{\min} \geq 1$ explore

$$\log_2 \frac{a_{\min}}{\sigma_w} = 0.0, 0.1, \ldots, 2.1, \;, \quad \log_2 \frac{a_{\max}}{\sigma_w} = 2.0, 2.1, \ldots, 4.1, \quad \text{with} \quad \sigma_w = 7 \text{ pixels}$$

and select $[a_{\min}, a_{\max}]$ if and only if

- weighted standard deviation across q of the $\widehat{h}(q)$ estimated from $a_{\min}$ to $a_{\max}$

$$\text{sd}_w < 0.06$$

$\Longrightarrow$ excludes multifractal scaling

q	-2	-1.5	-1	-0.5	-0.3	-0.2	-0.1	0	0.1	0.2	0.3	0.5	1	1.5	2	2.5	3
w	0.1	0.5	1	3	5	7	9	10	9	8	7	5	3	2	1	0.5	0.2

Patch-wise fractal analysis of mammographic breast tissue

For **each** patch of 360×360 pixels, i.e., 15.5×15.5 mm

$$\text{roughness: } h(q) = \lim_{a \to 0^+} \frac{h(q,a)}{\ln a}; \qquad \text{singularity spectrum: } \mathcal{D}(q,a) = \lim_{a \to 0^+} \frac{\mathcal{D}(q,a)}{\ln a}$$

$\Longrightarrow$ linear regressions $h(q,a)$ vs. $\log_2(a)$ and $\mathcal{D}(q,a)$ vs. $\log_2(a)$ across $[a_{\min}, a_{\max}]$

The Autofit Methodology: imposing $\log_2 a_{\max} - \log_2 a_{\min} \geq 1$ explore

$$\log_2 \frac{a_{\min}}{\sigma_w} = 0.0, 0.1, \ldots, 2.1, \;, \quad \log_2 \frac{a_{\max}}{\sigma_w} = 2.0, 2.1, \ldots, 4.1, \quad \text{with} \quad \sigma_w = 7 \text{ pixels}$$

and select $[a_{\min}, a_{\max}]$ if and only if

- weighted average of goodness of fit of $\widehat{h}(q)$ estimated from $a_{\min}$ to $a_{\max}$

$$\langle R_w^2 \rangle > 0.96$$

$\Longrightarrow$ ensures self-similarity

q	-2	-1.5	-1	-0.5	-0.3	-0.2	-0.1	0	0.1	0.2	0.3	0.5	1	1.5	2	2.5	3
w	0.1	0.5	1	3	5	7	9	10	9	8	7	5	3	2	1	0.5	0.2

Patch-wise fractal analysis of mammographic breast tissue

For **each** patch of 360×360 pixels:

$\Longrightarrow$ linear regressions $h(q,a)$ vs. $\log_2(a)$ and $\mathcal{D}(q,a)$ vs. $\log_2(a)$ across $[a_{\min}, a_{\max}]$

The Autofit Methodology: imposing $\log_2 a_{\max} - \log_2 a_{\min} \geq 1$ explore 418 couples

$$\log_2 \frac{a_{\min}}{\sigma_w} = 0.0, 0.1, \ldots, 2.1, \;, \;\; \log_2 \frac{a_{\max}}{\sigma_w} = 2.0, 2.1, \ldots, 4.1, \;\; \text{with} \;\; \sigma_w = 7 \text{ pixels}$$

and select $[a_{\min}, a_{\max}]$ if and only if

- $-0.2 < h(q=0) < 1$: expected roughness
- $1.7 < \widehat{D} < 2.5$: expect 2
- $R^2 > 0.96$: accurate estimation of H
- $sd_w < 0.06$: monofractal scaling
- $\langle R_w^2 \rangle > 0.96$: $h(q,a)$ sufficiently linear

$\Longrightarrow$ If no scale range $[a_{\min}, a_{\max}]$ for which all conditions are satisfied: **no scaling**.

Wavelet leader coefficients (Wendt et al., 2009, Sig. Process.)

- $H < 1/2$ monofractal anti-correlated: fatty tissues (healthy)
- $H > 1/2$ monofractal long-range correlated: dense tissues (healthy)
- $H \simeq 1/2$ monofractal uncorrelated: disrupted tissues (tumorous)

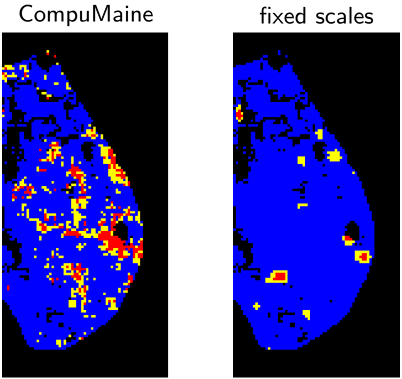

$$[a_{\min}, a_{\max}] = [2^3, 2^5]$$

Wavelet leader coefficients (Wendt et al., 2009, Sig. Process.)

- $H < 1/2$ monofractal anti-correlated: fatty tissues (healthy)
- $H > 1/2$ monofractal long-range correlated: dense tissues (healthy)
- $H \simeq 1/2$ monofractal uncorrelated: disrupted tissues (tumorous)

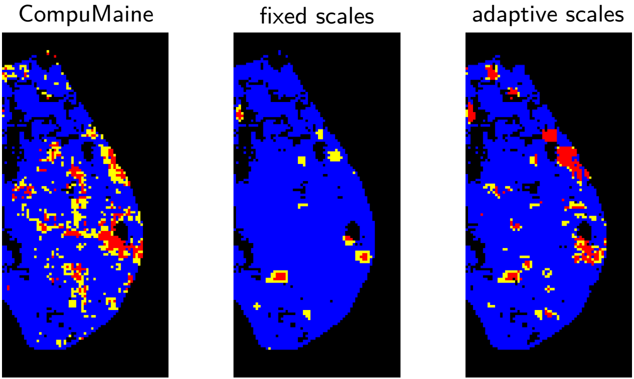

$[a_{\min}, a_{\max}] = [2^3, 2^5]$ $[a_{\min}, a_{\max}] \subset [2^2, 2^8]$

Wavelet leader coefficients (Wendt et al., 2009, Sig. Process.)

- $H < 1/2$ monofractal anti-correlated: fatty tissues (healthy)
- $H > 1/2$ monofractal long-range correlated: dense tissues (healthy)
- $H \simeq 1/2$ monofractal uncorrelated: disrupted tissues (tumorous)

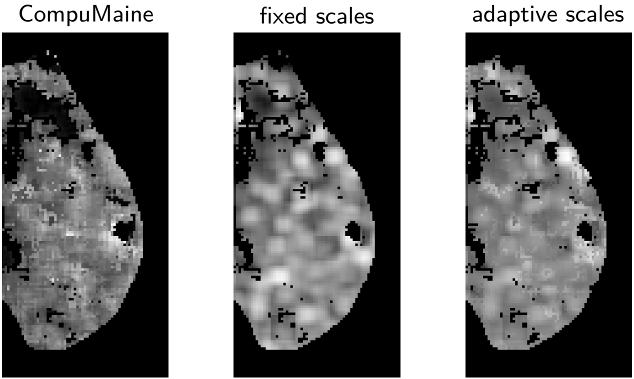

$[a_{\text{min}}, a_{\text{max}}] = [2^3, 2^5]$ $[a_{\text{min}}, a_{\text{max}}] \subset [2^2, 2^8]$

Marin et al., 2017, *Phys. Med. Biol.*

DDSM: *University of South Florida*, Digital Database for Screening Mammography

43 normal vs. 49 cancer, 35 benign

$\Longrightarrow$ digitized films: lossless LJPEG 12-bit images (pixel values: integers in $[0, 4095]$)

Tumorous breasts have more disrupted tissues compared to normal breasts:

normal vs. cancer: $P \sim 0.0023$, normal vs. benign: $P \sim 0.0049$.

Marin et al., 2017, *Phys. Med. Biol.*

DDSM: *University of South Florida*, Digital Database for Screening Mammography

43 normal vs. 49 cancer, 35 benign

$\Longrightarrow$ digitized films: lossless LJPEG 12-bit images (pixel values: integers in $[0, 4095]$)

Tumorous breasts have more disrupted tissues compared to normal breasts:

normal vs. cancer: $P \sim 0.0023$, normal vs. benign: $P \sim 0.0049$.

Gerasimova-Chechkina et al., 2021, *Front. Physiol.*

Russian: *Perm Regional Oncological Dispensary*

81 cancer vs. 23 benign

$\Longrightarrow$ digitally acquired mammograms: uncompressed 8-bit BMP images ($[0, 255]$)

Cancerous breasts have more disrupted tissues compared to breasts with benign lesions:

cancer vs. benign: $P \sim 0.003$

Marin et al., 2017, *Phys. Med. Biol.*

DDSM: *University of South Florida*, Digital Database for Screening Mammography

43 normal vs. 49 cancer, 35 benign

$\Longrightarrow$ digitized films: lossless LJPEG 12-bit images (pixel values: integers in $[0, 4095]$)

Tumorous breasts have more disrupted tissues compared to normal breasts:

normal vs. cancer: $P \sim 0.0023$,   normal vs. benign: $P \sim 0.0049$.

Gerasimova-Chechkina et al., 2021, *Front. Physiol.* $\Longrightarrow$ shared with us, with analyses

Russian: *Perm Regional Oncological Dispensary*

81 cancer vs. 23 benign

$\Longrightarrow$ digitally acquired mammograms: uncompressed 8-bit BMP images ($[0, 255]$)

Cancerous breasts have more disrupted tissues compared to breasts with benign lesions:

cancer vs. benign: $P \sim 0.003$

Patch-wise fractal analysis of mammographic breast tissue

Wavelet leader coefficients (Wendt et al., 2009, Sig. Process.)

- $H < 1/2$ monofractal anti-correlated: fatty tissues (healthy)
- $H > 1/2$ monofractal long-range correlated: dense tissues (healthy)
- $H \simeq 1/2$ monofractal uncorrelated: disrupted tissues (tumorous)

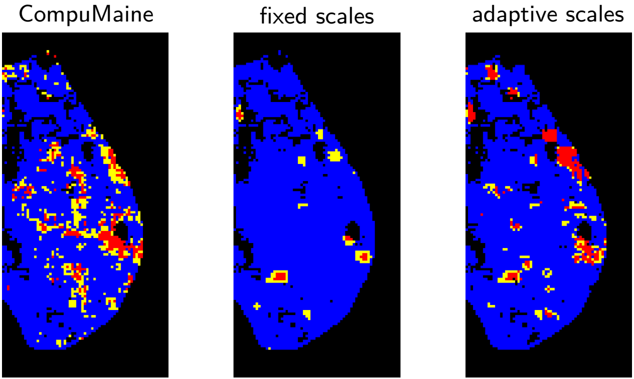

$[a_{\min}, a_{\max}] = [2^3, 2^5]$ $[a_{\min}, a_{\max}] \subset [2^2, 2^8]$

Mammogram datasets

Gerasimova-Chechkina et al., 2021, *Front. Physiol.* $\Longrightarrow$ shared with us, with analyses

Russian: *Perm Regional Oncological Dispensary*

81 cancer vs. 23 benign

$\Longrightarrow$ digitally acquired mammograms: uncompressed 8-bit BMP images ($[0, 255]$)

Cancerous breasts have more disrupted tissues compared to breasts with benign lesions:

cancer vs. benign: $P \sim 0.003$

Gerasimova-Chechkina et al., 2021, *Front. Physiol.* $\Longrightarrow$ shared with us, with analyses

Russian: *Perm Regional Oncological Dispensary*

81 cancer vs. 23 benign

$\Longrightarrow$ digitally acquired mammograms: uncompressed 8-bit BMP images ($[0, 255]$)

Cancerous breasts have more disrupted tissues compared to breasts with benign lesions:

$\underline{\text{cancer vs. benign:}}$ $P \sim 0.003$

Patch-wise analysis with wavelet leaders

- Daubechies wavelets with $n_\Psi = 2$ vanishing moments
- $\sim$ scales selected by the CompuMaine autofit method, up to rounding errors

Gerasimova-Chechkina et al., 2021, *Front. Physiol.* $\Longrightarrow$ shared with us, with analyses

Russian: *Perm Regional Oncological Dispensary*

81 cancer vs. 23 benign

$\Longrightarrow$ digitally acquired mammograms: uncompressed 8-bit BMP images ([0, 255])

Cancerous breasts have more disrupted tissues compared to breasts with benign lesions:

cancer vs. benign: $P \sim 0.003$

Patch-wise analysis with wavelet leaders

- Daubechies wavelets with $n_\Psi = 2$ vanishing moments
- $\sim$ scales selected by the CompuMaine autofit method, up to rounding errors

cancer vs. benign: $P \sim 0.074$

Patch-wise fractal analysis of mammograms with WT modulus maxima method

- disrupted tissues, characterized by $H \sim 1/2$, indicate loss of homeostasis
- quantity of disrupted tissues discriminates between

  (Marin et al., 2017) tumorous vs. normal $P \sim 0.0006$

  (Gerasimova-Chechkina et al., 2021) cancer vs. benign $P \sim 0.0030$

$\Longrightarrow$ exploration of 418 couples of $(a_{\text{min}}, a_{\text{max}})$ for each patch and strict conditions

Patch-wise fractal analysis of mammograms with WT modulus maxima method

- disrupted tissues, characterized by $H \sim 1/2$, indicate loss of homeostasis
- quantity of disrupted tissues discriminates between

  (Marin et al., 2017) tumorous vs. normal $P \sim 0.0006$

  (Gerasimova-Chechkina et al., 2021) cancer vs. benign $P \sim 0.0030$

$\Longrightarrow$ exploration of 418 couples of $(a_{\text{min}}, a_{\text{max}})$ for each patch and strict conditions

Reproduction with wavelet leaders formalism on Russian dataset

- range of scales for each patch extracted from CompuMaine analyses,
- remains less informative: $P \sim 0.0740$

Perspectives

From patch-wise to pixel-wise fractal analysis

- using wavelet leaders framework,
- combined with variational methods,
- with PyTorch implementation to benefit from fast GPU computing,
- reduced number of hyperparameters & fine-tuned automatically

$\Longrightarrow$ increase the sensibility in the measurement of the quantity of disrupted tissues

Perspectives

From patch-wise to pixel-wise fractal analysis

- using wavelet leaders framework,
- combined with variational methods,
- with PyTorch implementation to benefit from fast GPU computing,
- reduced number of hyperparameters & fine-tuned automatically

$\Longrightarrow$ increase the sensibility in the measurement of the quantity of disrupted tissues

Asymmetry in tissue disruption in cancerous cases

- assessed both in Marin et al., 2017 and Gerasimova-Chechkina et al., 2021,
- to be evaluated with (pixel-wise) wavelet leader fractal analysis

Perspectives

From patch-wise to pixel-wise fractal analysis

- using wavelet leaders framework,
- combined with variational methods,
- with PyTorch implementation to benefit from fast GPU computing,
- reduced number of hyperparameters & fine-tuned automatically

$\Longrightarrow$ increase the sensibility in the measurement of the quantity of disrupted tissues

Asymmetry in tissue disruption in cancerous cases

- assessed both in Marin et al., 2017 and Gerasimova-Chechkina et al., 2021,
- to be evaluated with (pixel-wise) wavelet leader fractal analysis

Anisotropic Gaussian fields for mammogram modeling

- observed in Richard & Biermé, 2010
- many tools that have never been applied to mammogram yet!